Chapter 5

Structure of cationic-surfactant – polyelectrolyte complexes

5.1 Introduction

This chapter deals with the structures exhibited by surfactant-polyelectrolyte complexes in aqueous solutions. Earlier work on the structure and phase behaviour of similar complexes is described in section 5.2. Our experimental results from optical microscopy and x-ray diffraction studies on complexes of cetyltrimethylammonium bromide (CTAB) with a variety of polyelectrolytes listed in table 5.1 are discussed in section 5.3. All complexes form a hexagonal phase, though with different lattice parameters depending on the polyelectrolyte used. There has not been any systematic study of the influence of the micellar shape on the structure of these complexes. Hence as in the case of CTAB-DNA complexes, discussed in chapter 3, we have tuned the micellar shape using sodium-3-hydroxy-2-naphthoate (SHN). Section 5.4 deals with the structural changes of complexes of CTAB-SHN with different polyelectrolytes on varying the SHN concentration. A transition from a hexagonal to a centered rectangular structure is observed in CTAB-SHN-PAA and CTAB-SHN-PGA complexes on increasing α (= [SHN]/[CTAB]). CTAB-SHN-PSS complexes show a transition from a hexagonal to a primitive rectangular structure as α is increased. They also show yet another structure at higher α, which has not yet been identified. Complexes of PVS with CTAB-SHN exhibit a a hexagonal $\rightarrow$ centered rectangular $\rightarrow$ lamellar transformation on increasing α. We have also examined complexes of these polyelectrolytes with the

double-tailed cationic surfactant didodecyldimethylammonium bromide (DDAB). The phase behaviour of the DDAB-water system and earlier work on complexes formed by DDAB with PGA are dealt with in section 5.5 . Our experimental results on DDAB-polyelectrolyte complexes are also discussed here. As discussed in section 5.6.1, our results on CTAB-SHN-polyelectrolyte complexes suggest the importance of poly-ion specificity in determining their structures. All DDAB-polyelectrolyte complexes exhibit a lamellar phase but the lattice parameter varies depending on the polyelectrolyte used. We also find that the weight fraction of the surfactant is the highest in PSS complexes and the least in DNA complexes. A similar trend is also seen in complexes of polyelectrolytes with CTAB as well as CTAB-SHN. This helps us to establish a correlation between the structure of the complexes and that of the surfactant-water system at similar surfactant content as discussed in section 5.6.2. Finally in section 5.7, we state the conclusions that can be drawn from the experiments discussed in this chapter.

5.2 Earlier studies

The complex formation between proteins and cationic detergents was first reported by Kuhn in 1940 [1, 2]. Later it was found to be a general phenomenon for anionic polyelectrolytes [3]. These complexes dissolve in the presence of salt [4]. These observations were made use of in the purification of anionic polysachcharides from biological tissues. Some of the earlier studies involved monitoring the binding of surfactants to polyelectrolytes using surfactant-selective electrodes [5]. Later NMR spectroscopy [6], small angle neutron scattering (SANS) and fluorescence techniques [7] were used to probe the structures in polyelectrolyte-surfactant systems.

One of the detailed studies on the phase behaviour of surfactant-polyelectrolyte systems has been by Thalberg et al [8] on didodecyltrimethyl ammonium bromide (DTAB)-poly (acrylic acid) (NaPA)-water and DTAB-sodium hyaluronate (NaHy)-water systems. The

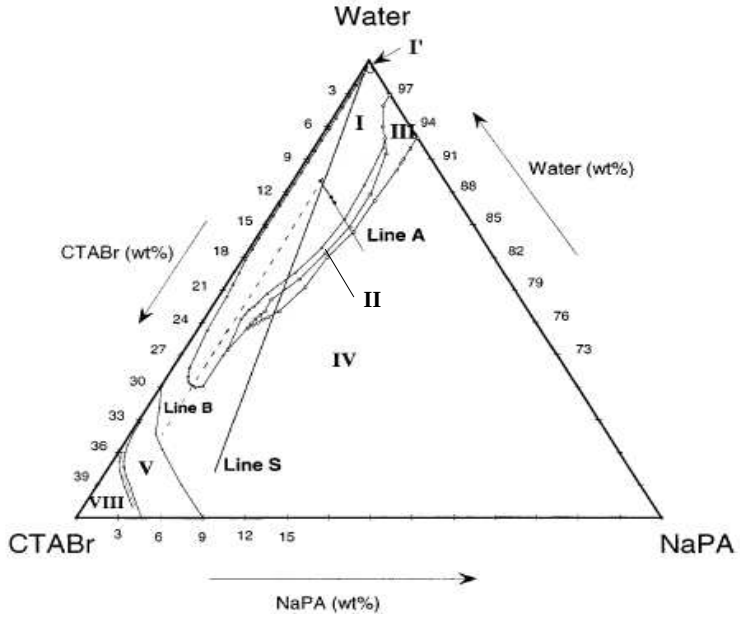

Figure 5.1: Phase diagram of CTAB-NaPA-water system [11].

complex formation occurs over a larger range of surfactant and polyelectrolyte concentration for complexes of DTAB with NaPA as compared to NaHy. Hence stronger interactions are indicated in NaPA complexes as compared to NaHy complexes, possibly due to the higher bare charge density of NaPA. The interactions in complexes of the anionic surfactant sodium dodecylsulphate (SDS) with cationic polyelectrolyte, poly(diallyldimethylammonium chloride) (PDADMAC) were found to be stronger than in the DTAB-NaPA system. This has been attributed to the smaller size of the surfactant head group of the anionic as compared to cationic surfactants [9, 10].

More detailed study of the phase behaviour of the CTAB-NaPA system has been carried out by Ilekti et al. [11, 12]. The phase diagram of NaPA-CTAB-water is given in fig 5.1. Dilute micellar solutions of CTAB with NaPA separate into a dilute aqueous phase and a concentrated mesophase containing the complex (cream phase) at the top (region I). Small angle diffraction studies indicate that these complexes have a hexagonal structure. The lattice parameter is in the range 5-6 nm, and is comparable to that of the hexagonal phase of CTAB-water system. At high dilutions (at surfactant concentrations close to CMC), a com-

plex with a cubic structure is obtained (region I'). A third phase appears between the cream and the aqueous phase on increasing the surfactant as well as polyelectrolyte concentration (region II). This is found to be an isotropic concentrated micellar phase. On further addition of NaPA the mesophase vanishes (region III). Finally the dilute aqueous phase vanishes at higher NaPA concentrations (region IV). At a fixed NaPA concentration along line B, the two phase region disappears at a surfactant concentration of $\sim 27\%$. CTAB-water system forms a hexagonal phase above 30% surfactant concentration. Between 30-37% the addition of polyelectrolyte leads to a hexagonal $\rightarrow$ nematic $\rightarrow$ micellar transition on increasing the polyelectrolyte concentration. Thus two opposite trends are exhibited in the dilute and concentrated CTAB solutions. The addition of NaPA to a dilute micellar solution leads to the phase separation of a concentrated mesophase, whereas the addition of the polyelectrolyte to a concentrated solution leads to the formation of an isotropic phase.

Thus on addition of NaPA to CTAB-water, three types of effects have been observed. i) The CTA^+ micelles retain their rod-like shape but the distances are collapsed (region I). ii) The distances remain the same but the shapes change. iii) Both the distances and the shapes change as seen in the cubic phase. The formation of a CTAB-NaPA complex involves the exchange of Br^- counter ion of CTAB with acetate (Ac^-) ion. Cetyltrimethylammonium acetate (CTAAc)-water system is known to form a cubic phase over a large range of surfactant concentration. It has a body-centered cubic unit cell, with large micelles at the apexes and center of a cube and pairs of smaller anisotropic micelles at the centers of the faces [13]. The formation of the cubic phase in dilute CTAB-NaPA solution can, therefore, be attributed to the nearly complete exchange of the Br^- and Ac^- ions. At higher surfactant contents when the ion exchange is less, a hexagonal phase is observed. The decrease in the inter-micellar distance can be understood in terms of the formation of polyion bridges between the micelles. Thus these studies show that the sequence of phases in these ternary systems is determined by the extent of counter ion exchange and by the water content.

Some studies have also probed the structures of these complexes when dried. It is found that stable membranes can be made from these dry complexes. The chain melting transition of the bilayers in the complex was found to shift to higher temperatures on drying. The permeability of these membranes can be modulated by small electric fields [14]. They are found to dissolve in organic solvents where they exhibit polyelectrolyte behaviour. X-ray investigations on the alkyltrimethylammonium bromide-poly (styrene sulfonate) (PSS) dry complexes reveal a lamellar phase with a periodicity ranging from 2.9 nm to 4.1 nm depending on the alkyl chain length of the surfactant. The ability to form liquid crystalline phases and their high solubility in organic solvents make them suitable materials for optoelectronics, ion separation membranes and molecular composites. A lamellar phase has also been reported in dry complexes of CTAB and dodecyltrimethylammonium bromide (DTAB) with PGA [15]. On heating, the complexes are found to be stable up to 150°C.

There have also been a few investigations on the structures of complexes formed by cationic surfactants with polyelectrolyte gels [16]. The structures of DTAB with cross-linked NaPA gels have been probed using small angle x-ray scattering (SAXS). The surfactant aggregation number and the ordering of micelles were investigated using time resolved fluorescence quenching. The surfactant concentration was kept well below the critical micellar concentration (CMC). A collapse of the gel was observed on increasing the CTAB concentration. Above a critical concentration, a *Pm*3*n* cubic phase was observed. On increasing the surfactant concentration above CMC, a hexagonal order was found in the 2D collapsed gel. The aggregation number was found to increase from 50 to 100 on increasing the surfactant concentration. This indicated that the aggregates that were initially globular formed short rods, at higher concentrations.

A more detailed study has been carried out on complexes of cationic surfactants with gels of anionic polyelectrolytes such as PSS and poly(sodium methacrylate) (PMAA) [17]. It was found that the alkyl chain length of the surfactant influences the formation of highly ordered

structures such as body-centred cubic (*bcc*), face-centred cubic (fcc) and hexagonal close packed (*hcp*), inside polyelectrolyte gel-surfactant complexes. The influence of bare charge density of the polyelectrolyte as well as the alkyl chain length of the surfactant on the structure of the complex was investigated. The longer the alkyl chain of the surfactant, stronger the hydrophobic interactions. However, the mesh size of the the gel was found to hinder the long alkyl chain (n=18) surfactants from forming well-ordered structures. At lower bare charge densities, longer alkyl chain surfactants were required to form highly ordered structures. The alkyltrimethylammonium bromide-PSS complexes formed a 2D hexagonal lattice indicating that the aggregates in the complex were composed of cylinders. It was concluded from these studies that surfactant aggregates bound by stiff polymer chains formed cylinders whereas those bound by flexible polymer chains formed spheres.

The influence of cationic polyelectrolytes of different charge densities on anionic surfactants has also been studied using SAXS [18]. Lamellar-lamellar coexistence with two distinct periodicities is observed when the polyelectrolyte is weakly charged, over a wide range of surfactant concentration. Similarly at high charge densities a lamellar phase, where the bilayers are closely packed, coexists with the regular lamellar phase whose periodicity varies with surfactant concentration. The coexistence is absent for intermediately charged polyelectrolyte and for nonionic polymers. Two possible modes of adsorptions of the polyelectrolyte on the bilayers have been proposed to account for this behaviour. Assuming the charge distribution along the polymer backbone to be non-uniform, the highly charged polymer segments are proposed to adsorb flat on the bilayer surface, whereas the segments with low charge density adsorb in loop-like conformation.

The complexes of cationic starch with anionic surfactants are also found to yield a variety of phases like cubic, hexagonal and lamellar [19]. In these studies the variable parameters were the alkyl chain length of the surfactant and the bare charge density of the polyelectrolyte. The effect of temperature on the structure of these complexes was also investigated.

It was found that the liquid crystalline phases are formed in the same sequence and with similar structures in the polyelectrolyte-surfactant-water system as in the surfactant-water system. Increase in the alkyl chain length leads to a sequence of structures ranging from a disordered micellar $\rightarrow$ *hcp* $\rightarrow$ *bcc* $\rightarrow$ hexagonal $\rightarrow$ lamellar phase. A similar sequence of transitions are obtained in the surfactant-water system by increasing the concentration of the surfactant. Increasing the temperature and decreasing the charge density of the polyelectrolytes in the complex were found to have similar effects on the structure of the complex. SANS studies indicate that the cationic starch has a helical conformation. When they associate with surfactants, more compact cylindrical aggregates are formed in which a core of surfactant is surrounded by the helical chains of cationic starch [20].

As discussed above, there have been several studies on the structures of polyelectrolyte-surfactant systems. However, the influence of the shape of the aggregates on the structure of the complex has not been probed systematically in any of these systems. Hence we have tuned the spontaneous curvature of the micelles in the dilute surfactant solution and examined the role of the aggregate morphology on the structure of the complex. This has been achieved using SHN which transforms CTAB aggregates from cylinders to bilayers, as described in chapter 2. The structure of the complex could also be specific to the chemical nature of the polyion. Not many of the earlier studies examined these systems from this perspective. Hence using four polyelectrolytes, which differ widely in the chemical nature of their charge moieties, bare charge density and persistence length, in addition to the single and double stranded DNA (discussed in chapter 3), we have made a comparative study of the structures of the complexes obtained in dilute solution of CTAB-SHN.

5.3 CTAB-polyelectrolyte complexes

A 10 mM CTAB solution was prepared and the polyelectrolyte was then added to it (table 5.1). Complexes, which precipitate out, were left in the solution for two days. The

Table 5.1: The bare charge densities and persistence lengths of the polyelectrolytes used, namely, double stranded (ds) DNA, single stranded (ss) DNA, poly (glutamic acid) (PGA), poly (acrylic acid) (PAA), poly (vinyl sulfonate) (PVS), poly (styrene sulfonate) (PSS).

Polyelectrolyte	bare charge density	l_p (nm)
ds DNA	1 $\overline{e}$/ 0.17 nm	50
ss DNA	1 $\overline{e}$/ 0.59 nm	1.5
PGA	1 $\overline{e}$/0.154 nm	2
PAA	1 $\overline{e}$/0.32 nm	1
PVS	1 $\overline{e}$/ 0.32 nm	1
PSS	1 $\overline{e}$/ 0.25 nm	10

precipitates were then transferred to a 1 mm glass capillary for x-ray diffraction studies. CTAB-polyelectrolyte complexes were found to be birefringent under a polarizing microscope. The complexes were prepared by varying the polyelectrolyte concentration ρ (= weight of CTAB/ weight of polyelectrolyte), above and below the isoelectric point ρ_{iso}, where the positive charges of the CTA^+ ions are balanced by the negative charges on the polyelectrolyte. The experimental observations were made at a temperature of 30°C.

X-ray diffraction studies on all four CTAB-polyelectrolyte complexes reveal three peaks in the small angle region (fig. 5.2). The scattering vectors are in the ratio 1:$\sqrt{3}$:2, which correspond to the (1 0), (1 1) and (2 0) peaks of a 2D hexagonal lattice. The lattice parameters are in general found to vary depending on the polyelectrolyte used. Though PVS and PSS complexes have similar lattice parameters, in CTAB-PVS complexes we obtain peaks corresponding to the (1 0), (2 0) and (2 1) reflections of a 2D hexagonal lattice (fig 5.2c). The lattice parameters and the peak positions for the different complexes are given in table 5.2. The effect of the polyelectrolyte and surfactant concentration on the lattice parameter was studied for CTAB- poly (glutamic acid) (PGA) complexes. The peak positions were found to be independent of ρ, and of CTAB concentration up to 100 mM . These observations are in broad agreement with the earlier experiments on CTAB-polyelectrolyte complexes in aqueous solutions [11, 17].

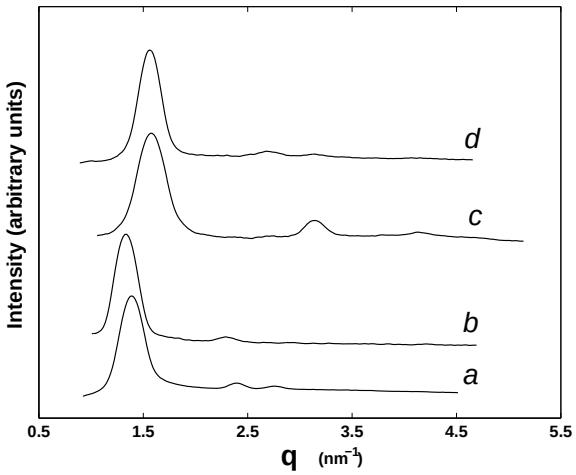

Figure 5.2: Diffraction patterns of the CTAB-polyelectrolyte complexes. ρ(= wt. of CTAB/wt of polyelectrolyte) and ρ_{iso} are 6.0, 3.88 for PAA (a); 1.8, 2.41 for PGA (b); 1.8, 1.78 for PSS (c); 1.15, 2.8 for PSS (d); CTAB concentration in the aqueous solution was 10 mM .

Table 5.2: The d-spacings, lattice parameters and structure of CTAB-polyelectrolyte complexes; *a* denotes the lattice parameter.

polyelectrolyte	$d_1(nm)$	$d_2(nm)$	$d_3(nm)$	$d_4(nm)$	*a*(nm)	structure
PAA	4.48	2.59	2.24		5.17	2-D hexagonal
PGA	4.61	2.67			5.33	2-D hexagonal
PSS	4.02	2.32	2.01		4.64	2-D hexagonal
PVS	4.0	2.31	2.0	1.52	4.64	2-D hexagonal

5.4 CTAB-SHN-polyelectrolyte complexes

Complexes were prepared using appropriate CTAB, SHN and polyelectrolyte concentrations. CTAB concentration was 10 mM. SHN concentration α (=[SHN]/[CTAB]), was varied from 0 to 0.7. The polyelectrolyte concentration ρ was varied over a wide range about the isoelectric point ρ_{iso}. The complexes were found to be birefringent under a polarizing microscope. X-ray diffraction studies of the complexes were carried out to probe their structure.

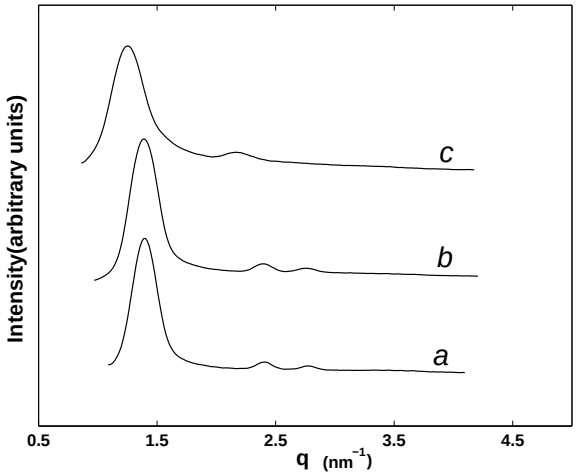

Figure 5.3: Diffraction patterns of the CTAB-SHN-PAA complexes in the hexagonal phase. α and ρ for the different curves are: 0.2, 6 (a); 0.2, 4 (b); 0.4, 0.6 (c), ρ_{iso}=4.85 at α=0.2; ρ_{iso}=6.47 at α=0.4; CTAB concentration in the aqueous solution was 10 mM .

In CTAB-SHN-PAA complexes, the diffraction patterns show three peaks in the small angle region, which can be indexed on a 2D hexagonal lattice (fig 5.3a). The hexagonal phase was found to occur up to α = 0.4. The peak positions remained independent of polyelectrolyte concentration above and below ρ_{iso} (fig 5.3a, b). The lattice parameter of the hexagonal phase however increases with SHN concentration (fig 5.3c). At α = 0.5, diffraction pattern shows additional peaks in the small angle region (fig. 5.4a) which could not be indexed on a hexagonal or a lamellar lattice. However, they could be indexed as the (2 0), (1 1) and (0 2) peaks of a centered rectangular lattice. Similarly, at α = 0.6, the x-ray diffraction pattern has 5 peaks in the small angle region (fig 5.4c). They could also be indexed as

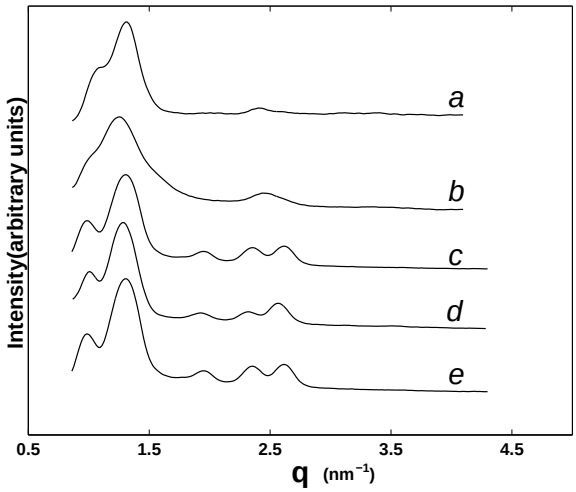

Figure 5.4: Diffraction patterns of the CTAB-SHN-PAA complexes. α and ρ for the different curves are: 0.5, 0.6 (a); 0.6, 0.6 (b); 0.6, 0.84 (c); 0.6, 12 (d); 0.7, 0.72 (e); ρ_{iso}=7.76 at α=0.5; ρ_{iso} =9.7 at α=0.6: ρ_{iso}=12.93 at α=0.7.

Table 5.3: The d-spacings, structure and lattice parameters of CTAB-SHN-PAA complexes at different values of α and ρ. *a* and *b* denote the lattice parameters. R denotes a phase with a centred rectangular lattice. The concentration of CTAB in the solution was 10 mM .

α	ρ_{iso}	ρ	$d_1(nm)$	$d_2(nm)$	$d_3(nm)$	$d_4(nm)$	$d_5(nm)$	phase	*a*(nm)	*b*(nm)
0	3.88	6	4.48	2.59	2.24			hexagonal	5.17	
0.2	4.85	0.6	4.38							
0.2	4.85	6	4.51	2.63	2.25			hexagonal	5.21	
0.4	6.47	0.6	4.88	2.99	2.67			hexagonal	5.64	
0.5	7.76	0.6	6.13	4.75		2.64	2.6	R	12.26	5.28
0.6	9.7	0.6	6.25	5.03		2.57				
0.6	9.7	0.84	6.45	5.03	3.34	2.76	2.50	R	12.90	5.52
0.6	9.7	12	6.27	4.84	3.24	2.66	2.39	R	12.54	5.32
0.7	12.93	0.72	6.23	4.86	3.27	2.70	2.43	R	12.66	5.40

the (2 0), (1 1), (3 1), (0 2) and (2 2) reflections from a 2D centered rectangular lattice. This was also true at α = 0.7 (fig 5.4e). The peak positions were found to be independent of the polyelectrolyte concentration and weakly dependent on SHN concentration (fig 5.4c, d). The peak positions and the lattice parameters for the various complexes are given in table 5.3.

For $\alpha < 0.5$, the CTAB-SHN-PGA complexes show three peaks in the small angle region with their q values in the ratio 1:$\sqrt{3}$:2 (fig 5.5a,b). These peaks could be indexed as the (1 0), (1 1) and (2 0) reflections of a 2D hexagonal lattice. The lattice parameter *a*, of the hexag-

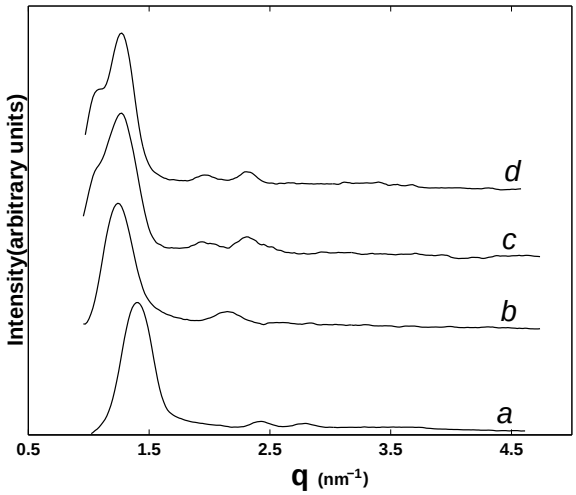

Figure 5.5: Diffraction patterns of the CTAB-SHN-PGA complexes. α and ρ for the different curves are: 0.2, 1.5 (a); 0.4, 1.93 (b); 0.5, 12 (c); 0.55, 0.72 (d); ρ_{iso}=3.02 at α=0.2; ρ_{iso}=4.02 at α=0.4; ρ_{iso}=4.82 at α=0.5; ρ_{iso}=5.36 at α=0.55;

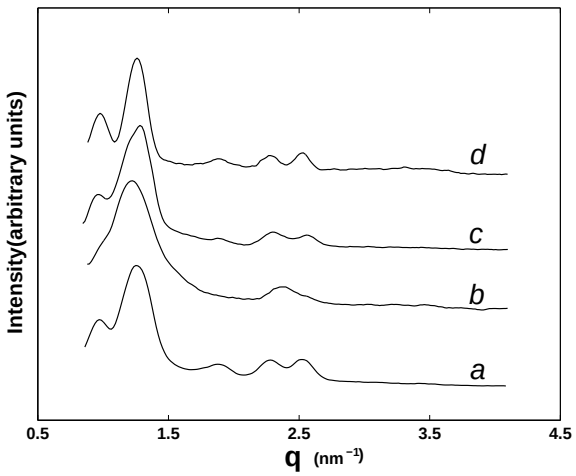

Figure 5.6: Diffraction patterns of the CTAB-SHN-PGA complexes. α and ρ for the different curves are: 0.6, 12 (a); 0.6, 1.8 (b); 0.6, 3.6 (c); 0.7, 6 (d); ρ_{iso}=6.0 at α=0.6; ρ_{iso}=8.0 at α=0.7;

Table 5.4: The d-spacings, structure and lattice parameters of CTAB-SHN-PGA complexes at different values of α and ρ. R denotes a phase with a centred rectangular lattice. *a* and *b* denote the lattice parameters.

α	ρ_{iso}	ρ	$d_1(nm)$	$d_2(nm)$	$d_3(nm)$	$d_4(nm)$	$d_5(nm)$	phase	*a*(nm)	*b*(nm)
0	2.41	1.8	4.61	2.66				hexagonal	5.33	
0.2	3.02	1.5	4.64	2.67	2.32			hexagonal	5.36	
0.4	4.02	1.93	5.06	2.92				hexagonal	5.84	
0.5	4.82	12.0	6.16	5.03	3.23	2.74		R	12.12	5.48
0.55	5.36	0.72	6.13	4.98	3.21	2.72		R	12.26	5.46
0.6	6.0	1.8	6.45	5.13		2.64				
0.6	6.0	3.6	6.43	4.96	3.32	2.75	2.48	R	12.86	5.48
0.6	6.0	12.0	6.45	4.90	3.32	2.75	2.48	R	12.9	5.48
0.7	8.0	6	6.33	4.98	3.30	2.75	2.49	R	12.46	5.5

onal structure gradually increases with α from 5.33 nm to 5.84 nm (table 5.4). Above α = 0.5, the peaks could be indexed as the (2 0), (1 1), (3 1) (0 2) and (2 2) reflections of a 2D rectangular lattice (fig 5.5 c,d). The peak positions in this phase was found to be independent of polyelectrolyte concentration (fig 5.6a,b). Similarly, the lattice parameters of this phase was only weakly dependent on SHN concentration (fig 5.6c,d). Similar trends are found in both the PAA and PGA complexes with the lattice parameters remaining insensitive to ρ and being weakly dependent on SHN concentration (table 5.3, 5.4). Hence the structures of CTAB-SHN-PGA complexes are similar to those of the PAA complexes.

A hexagonal phase is also observed in CTAB-SHN-PVS complexes for $\alpha < 0.4$ (fig 5.7a). The lattice parameter of the hexagonal lattice increases from 4.67 nm at α=0 to 5.16 nm for α = 0.2. At α=0.4, four peaks are observed in the small angle region which can be indexed as the (2 0),(1 1),(3 1) and (0 2) reflections of a 2D centered rectangular lattice (R) (fig 5.7b). The peak positions remain the same for α in the range 0.4 to 0.7 (fig 5.7b,c). At α = 0.7 and above, two peaks appear with the scattering vector q in the ratio 1:2 (fig 5.8a,b), corresponding to a lamellar structure. The position of the first order peak here remains the same as that of the (1 1) reflection seen at α = 0.6 (fig 5.7c). The lattice parameters of the different structures seen in this system are given in table 5.5.

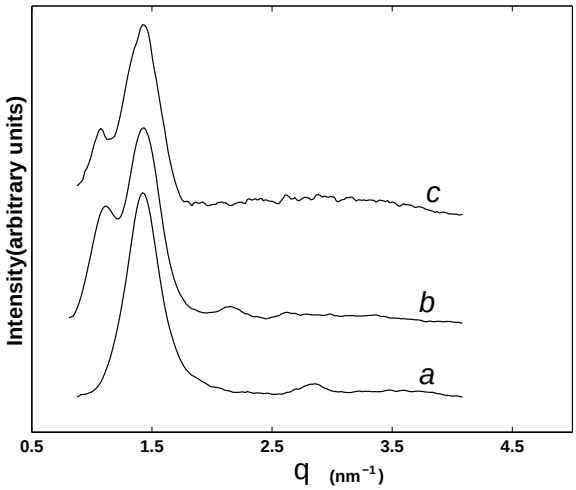

Figure 5.7: Diffraction patterns of the CTAB-SHN-PVS complexes.α and ρ for the different curves are: 0.2, 1.15 (a); 0.4, 1.15 (b); 0.6, 1.92 (c); ρ_{iso}=3.5 at α=0.2; ρ_{iso}=4.67 at α=0.4; ρ_{iso}=7.0 at α=0.6;

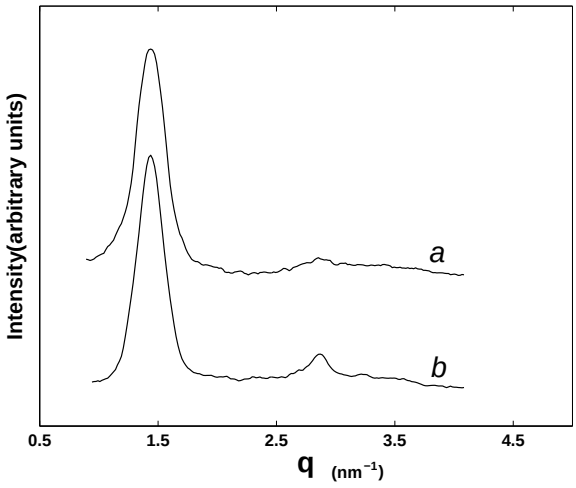

Figure 5.8: Diffraction patterns of the CTAB-SHN-PVS complexes. α and ρ for the different curves are: 0.7, 1.15 (a); 0.75, 1.15 (b); ρ_{iso}=9.33 at α=0.7; ρ_{iso}=9.99 at α=0.75;

Table 5.5: The d-spacings, structure and lattice parameters of CTAB-SHN-PVS complexes at different values of α and ρ. R denotes a phase with a centred rectangular lattice. *a* and *b* denote the lattice parameters.

α	ρ_{iso}	ρ	$d_1(nm)$	$d_2(nm)$	$d_3(nm)$	$d_4(nm)$	phase	*a*(nm)	*b*(nm)
0	2.8	1.15	4.00	2.31	2.00	1.52	hexagonal	4.6	
0.2	3.5	1.15	4.47		2.23				
0.4	4.67	1.15	5.67	4.37	2.93	2.37	R	11.34	4.74
0.5	5.6	1.15	5.67	4.47					
0.55	6.2	1.15		4.47					
0.6	7.0	1.92	5.85	4.34	2.17				
0.7	9.33	1.15	4.34	2.17			lamellar	4.34	
0.75	9.99	1.15	4.34	2.17			lamellar	4.34	

In CTAB-PSS complexes the diffraction patterns indicate that the structure of the complex remains hexagonal at low SHN concentration (fig 5.9a). At α = 0.4, four peaks are obtained in the small angle region that could not be indexed on a 2-D centered rectangular or a hexagonal lattice (fig 5.9b,c). The lamellar phase also had to be ruled out from the peak positions. Unlike in the centred rectangular phases of PAA , PGA or PVS complexes, the first peak was found to be more intense than the higher order peaks. The peaks could be indexed as the (2 0), (1 1), (2 1), (0 2), (3 1) and (4 1) reflections of a rectangular lattice corresponding to the plane group *pgg* (fig 5.9c). The peak positions of the *pgg* lattice, are sensitive to the SHN concentration. At a higher SHN concentration where α= 0.7, x-ray diffraction gives three peaks in the small angle region with no specific relationship between the values of q (fig 5.10). Additional peaks could not be observed even after very long exposures, and hence we have not been able to determine the structure of this phase. The peak positions in all these complexes are found to be independent of ρ. At α=0.75, we find that the complex dissolves for ρ above and below ρ_{iso}. The structures and the lattice parameters of CTAB-SHN-PSS complexes are given in table 5.6.

We have also studied the influence of these polyelectrolytes on dilute solutions of the

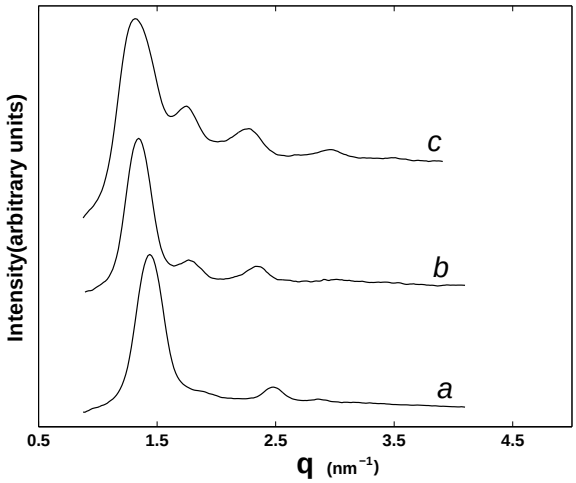

Figure 5.9: Diffraction patterns of the CTAB-SHN-PSS complexes. α and ρ for the different curves are: 0.2,2.25 (a); 0.5,3.6 (b); 0.6,4.5 (c); ρ_{iso}=2.23 at α=0.2; ρ_{iso}=3.56 at α=0.5; ρ_{iso}=4.45 at α=0.6;

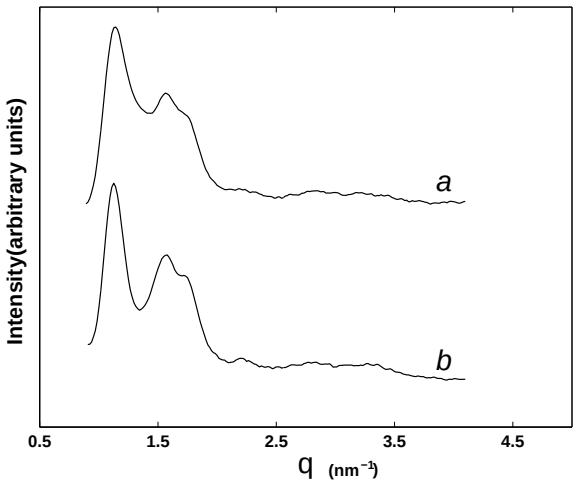

Figure 5.10: Diffraction patterns of the CTAB-SHN-PSS complexes. α and ρ for the different curves are: 0.7, 3.6 (a); 0.7, 12.0 (b); ρ_{iso}=5.93 at α=0.7.

Table 5.6: The d-spacings, structure and lattice parameters of CTAB-SHN-PSS complexes at different values of α and ρ. *a* and *b* denote the lattice parameters.

α	ρ_{iso}	ρ	d_1(*nm*)	d_2(*nm*)	d_3(*nm*)	d_4(*nm*)	phase	*a*(nm)	*b*(nm)
0	1.78	1.8	4.02	2.32	2.01		hexagonal	4.6	
0.2	2.23	2.25	4.37	2.53	2.18		hexagonal	5.04	
0.4	2.97	3	5.15						
0.5	3.56	3.6	4.67	3.46	2.68		*pgg*	9.34	5.36
0.6	4.45	4.5	4.84	3.56	2.77	2.14	*pgg*	9.68	5.54
0.7	5.93	3.6	5.58	4.02	3.59				
0.7	5.93	12	5.58	4.02	3.59				

double-tailed cationic surfactant didodecyldimethylammonium bromide (DDAB), which forms bilayers at all concentrations. Their structures are discussed below.

5.5 DDAB-polyelectrolyte complexes

5.5.1 Phase diagram of DDAB-water

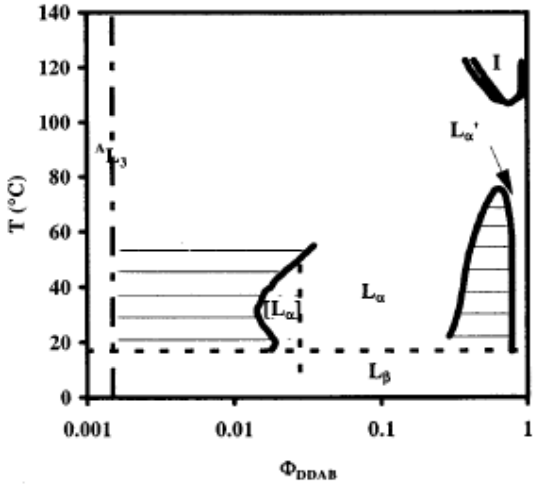

Figure 5.11: Phase diagram of DDAB-water system. L_α refers to the swollen lamellar phase. L'_α is the collapsed lamellar phase, L_β denotes the gel phase, and I the isotropic phase [21]

The phase diagram of the DDAB-water system has been studied extensively in the context of an anomalous attractive interaction between charged bilayers [21]. At low surfactant concentration the isotropic solution consists of unilamellar vesicles (L_3). The DDAB-water system is found to exhibit two coexisting lamellar phases at high surfactant concentration (fig 5.11). The lamellar phase (L_α) found at lower surfactant concentration shows the usual swelling behaviour given by

$$d = \delta_m/(1 - \phi_w) \tag{5.1}$$

Here d is the lamellar periodicity, δ_m the thickness of bilayer and ϕ_w the weight fraction of water.

On increasing the surfactant concentration, x-ray diffraction studies reveal in addition to the

lamellar peaks corresponding to L_α, peaks coming from a periodicity of 3.12 nm. The bilayer thickness of DDAB ~ 2.4 nm. Hence the second set of peaks correspond to a lamellar phase ($L_\alpha^{'}$) where the bilayers are collapsed with very little water between them. At 30^{o}C, there is a large region of coexistence of L_α and $L_\alpha^{'}$. On increasing the temperature the coexistence range decreases, leading to a critical point at 73^{o}C. In charged bilayer systems, the interactions between the bilayers is repulsive, owing to which the separation between the bilayers in the lamellar phase is determined by the water content. The appearance of a condensed phase ($L_\alpha^{'}$) at intermediate surfactant concentrations indicates that the interactions become attractive at these inter-bilayer separations. Such a behaviour has not been seen in other cationic surfactant systems like didodecyldimethylammonium chloride (DDACl)- water. Though the origin of the attractive interaction responsible for this behaviour is not known at present, they are suspected to arise from the condensation of Br^- counterions near the bilayer-water interface at these surfactant concentrations.

5.5.2 Earlier studies on DDAB-polyelectrolyte complexes

Mixtures of DDAB and the neutral lipid dilauroyl-sn-glycerophosphocholine (DLPC) form lamellar complexes with PGA [22]. By keeping ϕ_{PC} (= weight of neutral lipid/ total weight of the lipid) fixed and varying the PGA concentration, the lamellar periodicity remains constant at 5 nm. However at very low PGA concentrations ($\rho > \rho_{iso}$), faint additional peaks appear at small angles with d ~ 7 nm. On varying ϕ_{PC} from 0 to 0.9, keeping ρ fixed at ρ_{iso}, the d-spacing increases from 3.9 nm to 6 nm (fig 5.12). This behaviour was found to be independent of the molecular weight of the PGA used. Surprisingly no additional peaks corresponding to PGA-PGA correlation have been observed.

The thickness of DDAB-DLPC bilayers at ϕ_{PC} = 0.5 is nearly 3.14 nm. PGA molecules form a α-helix when complexed with cationic surfactants [23] with a diameter of 1.3 nm. Hence the lamellar periodicity of 5 nm is consistent with a bilayer thickness of ~ 3.2 nm

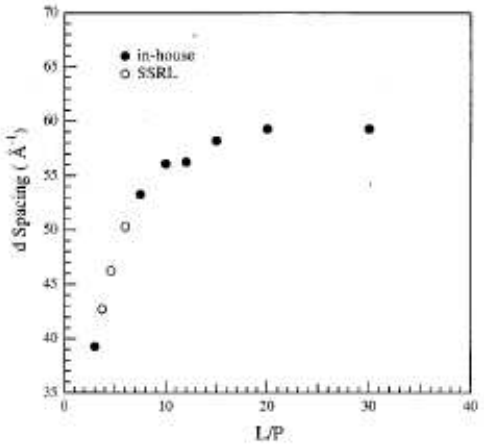

Figure 5.12: Plot of d spacing obtained as a function of L/P (= total weight of cationic and neutral lipid/ weight of PGA) [22].

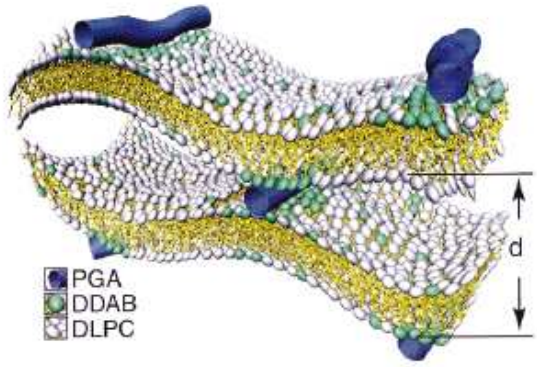

Figure 5.13: Schematic of the local lipid-PGA complex structure showing the 'pinching mechanism'. At larger length scales, the PGA macromolecules are positionally and orientationally disordered [22].

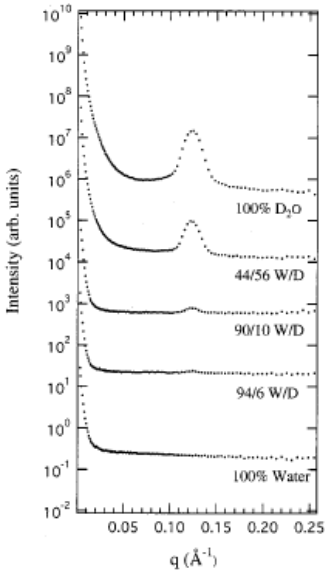

Figure 5.14: Small angle neutron scattering studies (SANS) data from DDAB-DLPC-PGA complexes at various solvent scattering densities [22].

and a PGA strand with two hydration shells ~ 1.8 nm. The swelling behaviour observed on increasing ϕ_{PC} at ρ_{iso} has been seen also in DDAB-DLPC-DNA system [24]. The increase in d-spacing on diluting the charge density of the bilayers, has led to the proposal of a pinched lamellar structure in these systems. This consists of locally pinched regions of DDAB and PGA with the d-spacing away from these regions determined by DLPC (fig 5.13). However the pinching mechanism proposed here has not been well established. PGA being flexible, with a persistence length $l_p \sim 2$ nm, a lamellar phase consisting of bilayers bridged by polyions cannot be ruled out.

Even if positional correlations exist between the PGA chains in the plane of the bilayer, the PGA-PGA peaks would be absent if there is no sufficient contrast between the PGA molecules and solvent. This can arise since the electron density of PGA molecules is nearly the same as that of water. However the contrast may be increased by using small angle neutron scattering techniques (SANS). Here the scattering length can be varied by changing the ratio of H_2O to D_2O. At high H_2O content, the scattering length of lipid and solvent are closely matched. Hence the scattering should be mainly from PGA molecules. However no

peaks are observed under these conditions (fig 5.14). On increasing the amount of D_2O, the contrast between the lipid and solvent increases, and a peak appears at 5 nm indicating the scattering from the lamellar complex.

Thus the structure in the lamellar phase of lipid-PGA systems are found to be different from those observed in lipid-DNA complexes. PGA strands, unlike the ds DNA, do not exhibit any order in the plane of the bilayer. Though PGA has a bare charge density comparable to that of ds DNA, its persistence length is an order of magnitude lower. Hence the absence of PGA-PGA correlations can be attributed to the low persistence length of PGA.

5.5.3 Structure of DDAB-polyelectrolyte complexes

All complexes appear as white precipitates phase separating out of the aqueous solution. They are found to be birefringent under a polarizing microscope. The complexes in general form a lamellar structure. In DDAB-ds DNA complexes the peak positions do not shift significantly on increasing the DNA concentration (fig 5.15b,c). Hence the lattice parameter of the DDAB-ds DNA complexes remain at 4.51 nm, nearly independent of DNA concentration on varying ρ across ρ_{iso}. However at high DNA concentration, a shoulder appears on the first order peak at 3.69 nm (fig 5.15c). A broad peak appears at 2.51 nm for ρ below ρ_{iso} (fig 5.15b). We have also studied the complexes formed by ss DNA with DTAB. The lamellar periodicity of these complexes is 4.15 nm (fig 5.15a).

The diffraction pattern of DDAB-PGA complexes give two peaks in the small angle region with their q values in the ratio 1:2, indicating a lamellar structure for the complex (fig 5.16a). These complexes have a periodicity of 3.82 nm for $\rho > \rho_{iso}$. On increasing the PGA concentration, the lattice parameter decreases to 3.43 nm for $\rho < \rho_{iso}$. The diffraction pattern of DDAB-PAA complexes also consists of two peaks (fig 5.16b) indicating a lamellar structure with a spacing of 3.46 nm for $\rho > \rho_{iso}$ and a spacing of 3.22 nm for $\rho < \rho_{iso}$. The x-ray

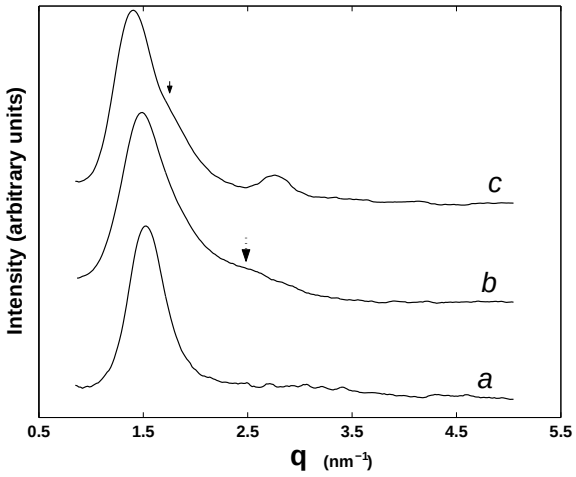

Figure 5.15: Diffraction patterns of the DDAB-DNA complexes. DDAB-ss DNA complex at ρ = 9.2 (a). DDAB-ds DNA complex with ρ = 9.2 (b); ρ=0.92 (c); ρ_{iso} = 0.71; The arrow in curve (b) indicates the peak due to the scattering from the helical structure of the DNA strand; The arrow in curve (c) indicates the DNA-DNA peak; DDAB concentration in the aqueous solution is 10 mM .

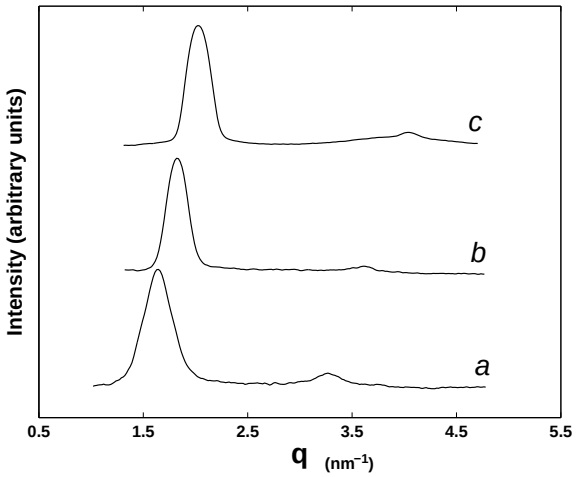

Figure 5.16: Diffraction patterns of : (a) DDAB-PGA complex at ρ = 9.2; ρ_{iso} = 3.07 , (b) DDAB-PAA complex at ρ = 0.92; ρ_{iso} = 4.59 , (c) DDAB-PVS complex at ρ = 0.92; ρ_{iso} = 3.57.

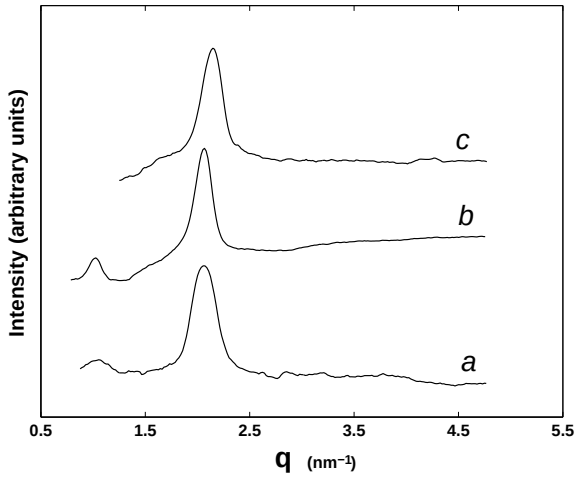

Figure 5.17: Diffraction patterns of DDAB-PSS complexes at different values of ρ. ρ = 4.6 (a); ρ = 2.2 (b); ρ = 1.25 (c). ρ_{iso} = 2.25. DDAB concentration in the aqueous solution is 10 mM .

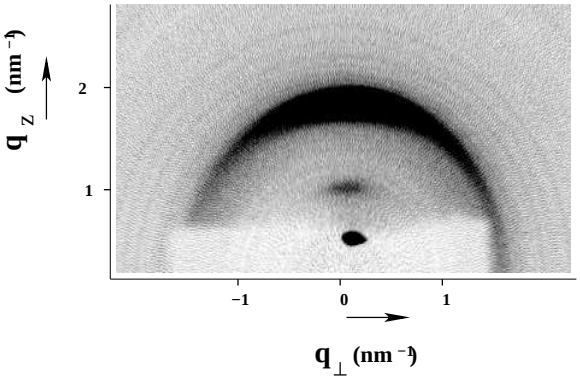

Figure 5.18: Diffraction pattern of a partially oriented DDAB-PSS complex; ρ = 1.65; ρ_{iso} = 2.25.

diffraction pattern of complexes of PVS with DDAB also give two peaks in the small angle region (fig 5.16c) showing a lamellar structure with the periodicity decreasing from 3.18 nm to 3.09 nm on increasing the PVS concentration.

The complexes of PSS with DDAB however show a very different behaviour. At $\rho > \rho_{iso}$, two peaks appear in the small angle region with no definite relationship between their q values (fig 5.17 a,b). The intensity of the peak at 5.95 nm is found to be lower than the peak at 3.03 nm. The peak at 5.95 nm remains nearly independent of the polyelectrolyte concentration. However at high PSS concentration, much below ρ_{iso}, the peak at 5.95 nm

Table 5.7: Relative intensities of the first peak (I_1) w.r.t the second peak (I_2) at different values of ρ in DDAB-PSS complexes. ρ_{iso} = 2.25.

ρ	I_1/I_2
9.01	0.01
4.6	0.048
3.1	0.027
2.2	0.063
1.65	0.029

Table 5.8: The d-spacings and lattice parameters of DDAB-polyelectrolyte complexes at various polyelectrolyte concentrations. d denotes the lattice parameter.

polyelectrolyte	ρ_{iso}	ρ	$d_1(nm)$	$d_2(nm)$	d (nm)
ds DNA	0.71	9.2	4.51	2.25	4.51
ds DNA	0.71	0.92	4.50	2.25	4.50
ss DNA	0.71	9.2	4.15		4.15
PGA	3.07	9.2	3.82	1.91	3.82
PGA	3.07	0.92	3.53	1.75	3.53
PAA	4.59	11.56	3.48		3.48
PAA	4.59	8.66	3.46	1.73	3.46
PAA	4.59	5.56	3.45	1.73	3.45
PAA	4.59	0.92	3.22		3.22
PVS	3.57	10.02	3.18		3.18
PVS	3.57	7.66	3.18		3.18
PVS	3.57	4.7	3.11		3.11
PVS	3.57	0.92	3.09		3.09
PSS	2.25	9.2	6.08	3.03	
PSS	2.25	4.6	5.96	3.03	
PSS	2.25	3.10	5.95	3.03	
PSS	2.25	2.20	6.22	3.04	
PSS	2.25	1.65	5.84	2.92	
PSS	2.25	1.25	2.99	1.50	2.99
PSS	2.25	0.9	2.96	1.48	2.96

disappears (fig 5.17c). In an oriented sample of DDAB-PSS complex (fig 5.18), the peaks occur at q_z = 1.04 nm^{-1} and at 2.12 nm^{-1}. No peaks appear along $q_\perp$ direction. On increasing the temperature up to 70 ^{o}C the peak positions remain at around 6 nm and 3.03 nm respectively. But on increasing the temperature to 75 ^{o}C, the peak at 6 nm disappears. Also no peaks could be observed due to the scattering from the supernatant, indicating that the peaks at 6.03 ± 0.1 nm and at 3.03 nm occur due to the scattering from the complex.

The relative intensities of the peaks were calculated after geometric corrections. The ratio of the intensity of the first peak with respect to the second, does not show any systematic variation with ρ (table 5.7). The inner peak seen in DDAB-PSS was not observed in any of the other DDAB-polyelectrolyte complexes studied, up to 8 nm which is the largest d-spacing that can be measured in our experimental set up. The d-spacings of the lamellar phase of all the DDAB- polyelectrolyte complexes are summarized in table 5.8.

5.6 Discussion

5.6.1 CTAB-SHN-polyelectrolyte complexes

All CTAB-polyelectrolyte complexes show a hexagonal phase. However the lattice parameters of the 2D hexagonal lattice vary, depending on the polyelectrolyte used. The diffraction pattern of CTAB-PVS and CTAB-PSS complexes indicate that though the lattice parameters remain almost the same for both the complexes, the electron density distribution is different.

Since PGA, PAA, PVS and PSS have very short persistence lengths (1-10 nm), the hexagonal phase of CTAB-SHN with the polyelectrolytes can be expected to consist of cylindrical micelles bridged by the polyelectrolyte chains (fig. 5.19). A similar structure has been proposed for the hexagonal phase of CTAB-PAA complexes earlier [11]. Since SHN is known to decrease the spontaneous curvature of cylindrical aggregates, the increase in the lattice

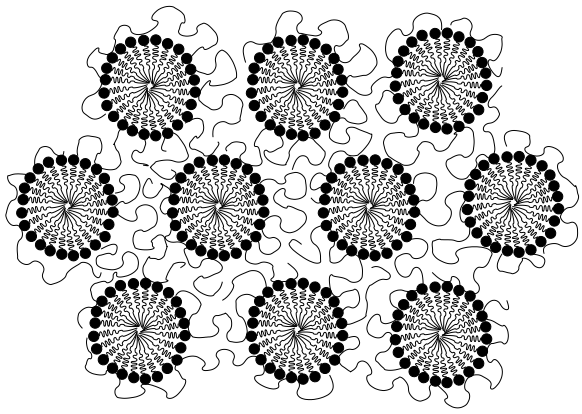

Figure 5.19: Schematic of the structure of the hexagonal phase of CTAB-polyelectrolyte complexes where the cylindrical micelles are bridged by the polymer chains.

parameters of hexagonal phase with SHN concentration can result from an increase in the size of the micellar cylinders. The lattice parameters of the hexagonal phase of the complex is similar to that observed in the hexagonal phase of CTAB-SHN with 50-60% water content (chapter 2, table 2.2).

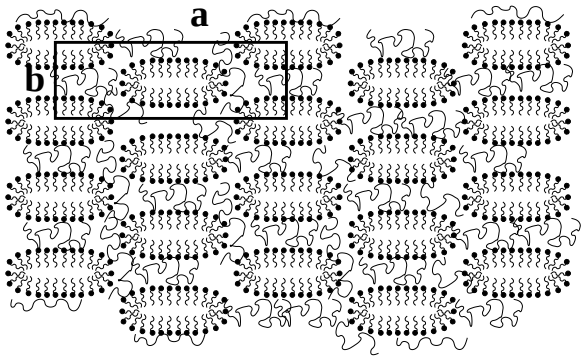

Figure 5.20: Schematic of the structure of the *cmm* phase of CTAB-SHN-PAA/PGA/PVS complexes where the ribbon-like surfactant aggregates are bridged by the polyelectrolyte chains.

The 2D centered rectangular lattice observed in CTAB-SHN-PGA complexes can arise if positional correlation develops between the PGA chains in the plane of the bilayers. However, as discussed in section 5.5.2, the neutron scattering experiments on DDAB-PGA complexes have shown that no positional correlations exist between the PGA strands in the plane of the bilayers [22]. The absence of such a correlation has been attributed to the low per-

sistence length of PGA. Hence positional correlation of the PGA strands can be ruled out in CTAB-SHN-PGA bilayers. Moreover, if such correlations exist, leading to the formation of a 2D lattice, the lattice parameters would depend on the PGA concentration. The lattice parameters in these complexes however remain independent of PGA concentration and are only weakly dependent on SHN concentration.

The structure of the centered rectangular phase observed at higher SHN concentrations in CTAB-SHN-PGA complexes is different from a similar phase observed in lipid-DNA complexes [25]. In cationic lipid-DNA complexes, a centered rectangular lattice arises from the transbilayer positional correlation of the DNA strands. Here, the lattice parameter corresponding to the separation between the DNA strands sandwiched between the bilayers, changes with the DNA concentration. Therefore, we propose a structure for the complexes of PGA with CTAB-SHN, consisting of ribbon-like aggregates arranged on a 2-D rectangular lattice (fig 5.20), corresponding to the plane group *cmm*. Such a phase has been observed earlier in some surfactant systems in between the hexagonal and lamellar phases and also in the CTAB-SHN-water system as described in Chapter 2 [26]. However it has not been observed in any of the earlier studies on polyelectrolyte-surfactant systems.

The lattice parameters of CTAB-SHN-PAA complexes do not vary with PAA concentration, but depend weakly on SHN concentration. They are similar to those of CTAB-SHN-PGA complexes, indicating that PAA and PGA complexes form similar structures. Hence we propose that CTAB-SHN-PAA complexes also form a rectangular phase consisting of ribbon-like aggregates bridged by the polymer chains (fig 5.20). The lattice parameters of these complexes are comparable to those observed in the ribbon phases of CTAB-SHN-water system (Chapter 2).

The lattice parameters of CTAB-SHN-PVS complexes also do not vary with PVS concentration and depend weakly on SHN concentration. The lattice parameters are different

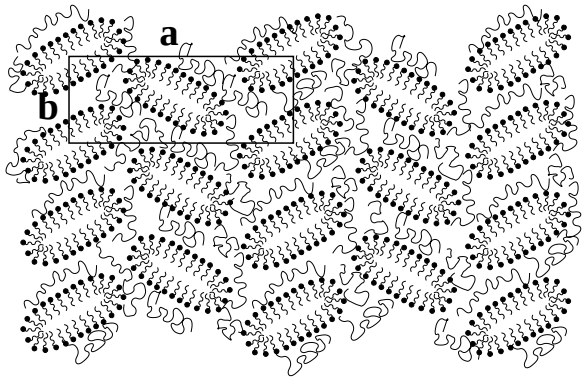

Figure 5.21: Schematic of the structure of the *pgg* phase of CTAB-SHN-PSS complexes where the ribbon-like surfactant aggregates are bridged by the polyelectrolyte chains.

from those observed in PAA and PGA complexes. The flexibility of PVS is however similar to that of PAA. Hence a PVS-PVS correlation cannot occur in the plane of the bilayers. Thus a ribbon phase similar to that seen in PAA and PGA complexes can be proposed for CTAB-SHN-PVS complexes characterized by a centred rectangular lattice.

The lattice parameters of CTAB-SHN-PSS complexes are weakly sensitive to SHN concentration and are independent of PSS concentration. This rules out a PSS-PSS correlation in the plane of CTAB-SHN bilayers. Hence the *pgg* structure of CTAB-SHN-PSS complexes at high SHN concentrations, most probably consists of ribbon-like aggregates bridged by polyelectrolyte chains (fig 5.21). Such structures have also been seen in some surfactant systems [27]. But we have not observed this in the CTAB-SHN-water system. Perhaps the complex is driven to form such structures because of their low water content. The phase observed in CTAB-SHN-PSS complexes at $\alpha = 0.7$, might also consist of ribbons arranged on an oblique lattice, a structure seen in sodium dodecylsulphate-water system [27].

The persistence length of a polyelectrolyte is very sensitive to counter-ion and salt concentrations [28]. Since most of the polyelectrolyte charges are neutralized in the complexes, the relevant quantity here is the intrinsic persistence length due to the stiffness of the polymer backbone. The persistence lengths of PGA, PAA, PSS and PVS are about 2, 1, 10 and 2 nm.

Table 5.9: Sequence of phase transitions in CTAB-SHN-Polyelectrolyte complexes on varying α.

polyelectrolyte	α	structure
PAA	0	2-D hexagonal
PAA	0.5	cmm
PAA	0.7	cmm
PGA	0	2-D hexagonal
PGA	0.5	cmm
PGA	0.7	cmm
PVS	0	2-D hexagonal
PVS	0.4	cmm
PVS	0.7	lamellar
PSS	0	2-D hexagonal
PSS	0.4	pgg
PSS	0.7	oblique?

They carry a bare charge of $1\bar{e}$/0.154 nm, $1\bar{e}$/0.32 nm, $1\bar{e}$/0.25 nm and $1\bar{e}$/0.154 nm respectively. In an earlier chapter of this thesis, we have seen that the complexes of CTAB-SHN with ds DNA and ss DNA, which have the same charge moiety but a persistence length that differ by almost to orders of magnitude, give similar structures at similar α. The complexes of CTAB-SHN with the polyelectrolytes, PAA and PVS which differ only by the chemical nature of the charge moiety exhibit a different sequence of transitions with α (table 5.9). However, PAA and PGA which have the same charge moiety but different bare charge densities and persistence lengths exhibit identical behaviour on varying α. Hence the structures seen in these complexes may not be primarily determined by the persistence length of the polyelectrolyte or its bare charge density. Similarly PSS and PVS exhibits different structures on varying α. Thus we find that the structures observed in these complexes are specific to each polyion. The theories of polyelectrolyte-surfactant complexation do not at present take into account the specificity of the polyion. Our results indicate that this needs to be incorporated to predict the variety of structures seen in these complexes.

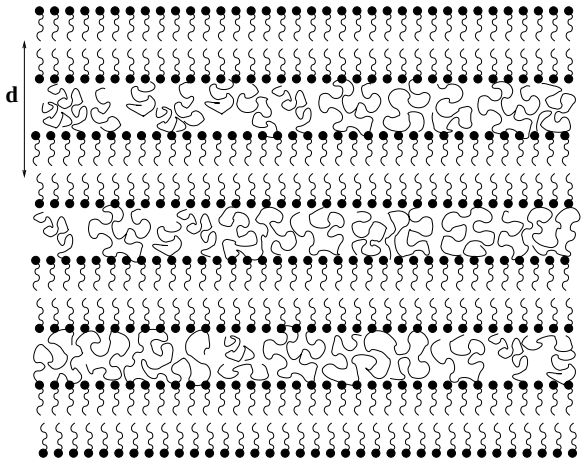

Figure 5.22: Lamellar phase of the complexes of flexible polyelectrolytes with DDAB. The bilayers are bridged by the flexible polymer chains

5.6.2 Structures in DDAB-polyelectrolyte complexes

Since DDAB always forms bilayers in aqueous solution [21], the lamellar phase of DDAB-DNA complexes is expected to consist of DNA sandwiched between bilayers; a structure similar to that seen in cationic lipid -DNA complexes (L_α^C). The lamellar periodicity of 4.51 nm for the DDAB-DNA complex is consistent with a DNA strand of diameter 2.5 nm, sandwiched between a bilayer of thickness 2 nm. The peak observed at 3.96 nm corresponds to the DNA-DNA peak (fig.5.15c). The hump at 2.51 nm appears due to scattering from the helical structure of the ds DNA strand (fig.5.15b).

The complexes of flexible polyelectrolytes with DDAB consists of bilayers bridged by the polyelectrolyte to form a lamellar structure (fig 5.22). The decrease in the lamellar periodicity when the polyelectrolyte concentration is below ρ_{iso}, could be the result of enhanced neutralization of the surfactant charges. The effective attraction between bilayers can also increase if more and more polyions bridge the bilayers when the polyelectrolyte concentration is increased. The bilayer periodicity of the various complexes (table 5.8) except for the single and double stranded DNA and PGA, is $\sim$ 3.2 nm, the periodicity observed in the condensed lamellar phase (L'_α) of the DDAB-water system. The absence of peaks corresponding to a correlation between the PAA, PGA or PVS strands is consistent with their persistence

length being ~ 1 nm; they remain disordered in the plane of the bilayers. Positional correlations between the polymer strands in the plane of the bilayers have been observed only for ds DNA strands whose persistence length is 50 nm [22].

The peak observed at 3.03 nm in DDAB-PSS complexes can arise due to scattering from the bilayers, if the complex forms a lamellar structure. This would lead us to surmise that the peak at smaller angles, corresponding to 6.03 ± 0.1 nm arises due to scattering from the PSS-PSS strands. We would then expect this peak position to shift with PSS concentration. However since the peak always appears at 6.03 nm, irrespective of the polyelectrolyte concentration, this possibility may be ruled out. In addition to this, we also find that when the sample is oriented, all the peaks appear along the q_z direction (fig 5.18). A PSS-PSS correlation peak, which arises from ordering in the plane of the bilayers would be oriented perpendicular to the lamellar peaks.

Due to the unique phase behaviour seen in DDAB-water system as discussed in section 5.5.1, it is possible that the complex forms two lamellar phases with distinct periodicities. But, to be consistent with the observations in the surfactant system, we would expect the peak position of the two coexisting lamellar phases in the complex, to shift with temperature (fig 5.11). However, the peak position is found to remain independent of temperature up to 73 ^{o}C, and then disappears. Moreover, if we assume that DDAB-PSS complex consists of two distinct lamellar phases, one would expect the scattering intensities corresponding to the two structures to vary with polyelectrolyte concentration. However the relative intensity of the inner peak with respect to the first order lamellar peak exhibits no particular dependence on ρ (table 5.7). The peak observed here at small angles has not been observed in any of the other polyelectrolyte complexes up to 8 nm.

The disappearance of the peak at high polyelectrolyte concentrations much below ρ_{iso}, is equally surprising. The dissolution of the complex at low salt concentrations (~ 50 mM

NaBr) indicates that the structure of the complex is highly sensitive to the presence of salt. Hence the structure of DDAB-PSS complex remains unexplained at present. More work is required to understand the structure exhibited by this complex.

5.6.3 Surfactant content of the various polyelectrolyte complexes

From the lattice parameters of the DDAB-polyelectrolyte complexes, we can estimate the surfactant content in the complexes. If δ_s is the bilayer thickness, d the lattice parameter, and if we assume that density of surfactant $\rho_s^{DDAB} \approx \rho_w$, the density of water, then the weight fraction of DDAB in the complex is $\phi_s^{DDAB} = \frac{\delta_s}{d}$. The bilayer thickness of DDAB in the complex , $\delta_s \sim 2$ nm. ϕ_s^{DDAB} calculated for the various complexes is given in table 5.10.

Similarly, we may also estimate the surfactant content of the hexagonal phase of CTAB-polyelectrolyte complexes. The radius of the CTAB cylinder, R_m is $\sim$ 1.98 nm [11]. A unit cell of a hexagonal lattice consists of one cylindrical micelle of CTAB. The ratio of the area occupied by the cylinder to the area of a unit cell obtained from the lattice parameter of the hexagonal lattice, gives the surfactant weight fraction. We assume here that density of CTAB, $\rho_s^{CTAB} \approx \rho_w$ and that the radius of the micellar cylinders in the complex do not change with surfactant concentration. Hence the surfactant content of the CTAB-polyelectrolyte complexes are given by, $\phi_s^{CTAB} = (2 \pi R_m^2) / \sqrt{3} a^2$. These values are also given in table 5.10.

At similar SHN concentrations ($\alpha = 0.7$) the lattice parameters of CTAB-SHN-PAA/PGA complexes were nearly the same as the lattice parameters observed at $\phi_s = 0.6$ in the CTAB-SHN-water system. The lattice parameters of the centred rectangular phase at these SHN concentrations are a = 13 nm, b = 5.4 nm. Assuming that the size of the surfactant aggregates in the complex remain the same as those in the surfactant system at similar lattice parameters, we could estimate the surfactant content of CTAB-SHN-polyelectrolyte complex at α = 0.7. Since PVS complexes form a lamellar phase at these SHN concentrations,

Table 5.10: Estimated surfactant content in complexes of polyelectrolytes with DDAB (ϕ_s^{DDAB}), CTAB (ϕ_s^{CTAB}) and CTAB-SHN (ϕ_s^{CS}). ϕ_s^{CS} corresponds to $\alpha = \sim 0.7$.

polyelectrolyte	ϕ_s^{DDAB}	ϕ_s^{CTAB}	ϕ_s^{CS}
ss DNA	0.48	0.48	0.58
PGA	0.52	0.5	0.6
PAA	0.58	0.53	0.61
PVS	0.63	0.66	0.69
PSS	0.66	0.66	

assuming a bilayer thickness of 3 nm for CTAB-SHN, we have estimated the surfactant content (see table 5.10).

Table 5.10 indicates that both CTAB and DDAB complexes exhibit similar behaviour. The surfactant content in the complex varies as ss DNA < PGA < PAA < PVS < PSS. Though the estimated surfactant content varies depending on the polyelectrolyte used, the structure remains the same for all the polyelectrolytes with the complex forming a hexagonal phase when the aggregates in the surfactant solution consists of cylinders (in the case of CTAB) and a lamellar phase when the surfactant solution consists of bilayers (in the case of DDAB). We need to note here that CTAB-water system consists of a hexagonal phase over a large range of surfactant concentration and DDAB forms only bilayers in aqueous solutions.

The behaviour observed above can be contrasted with the trends in CTAB-SHN-polyelectrolyte complexes. A variety of structures are observed in this system depending on the polyelectrolyte used. But if we estimate the water content in the CTAB-SHN-polyelectrolytes, for example at α (= [SHN]/[CTAB]) $\sim$ 0.7, they exhibit a trend (table 5.10) similar to the CTAB and DDAB complexes. The structures observed in the former vary depending on the polyelectrolytes used since the CTAB-SHN-water system at $\alpha \sim 0.7$, exhibits these structures at similar surfactant content (table 4, chapter 2). We have assumed here that for similar lattice parameters, the size of the surfactant aggregates remain the same in the complex as well as in the surfactant-water system.

Thus we find a correlation between the structure of the complex and the structure exhibited by the surfactant system at similar surfactant content. Such a correlation has not been suggested in any of the earlier studies; the use of a surfactant system with a very rich phase behaviour makes it possible in the present case.

5.7 Conclusions

We have studied in detail the influence of aggregate morphology on the structure of surfactant-polyelectrolyte complexes. This has been achieved by using SHN which tunes the spontaneous curvature of CTAB cylinders. For any given polyelectrolyte, the complex shows a variety of structures on varying α. We have obtained novel structures for the complexes, like *cmm* and *pgg*, which have not been reported in earlier studies. These studies show that the chemical nature of the polyion plays an important role in determining the structure of the complexes, by determining the surfactant content of the complex. We also found that the structure exhibited by the complex is almost identical to that seen in the corresponding surfactant system at similar surfactant concentration.

Bibliography

[1] E. D. Goddard and K. P. Ananthapadmanabhan (Editors), *Interactions of Surfactants with Polymers and Proteins* (CRC Press, Boca Raton) 1993.

[2] R. Kuhn, Ber. Dtsch. Chem. Ges. **73**, 1080 (1940)

[3] J. E. Scott, Chem. Ind. (London), 168 (1955).

[4] T. C. Laurent, and J. E. Scott, Nature **202**, 661 (1964)

[5] T. Gilanyi, and G. Wolfram, Colloids Surf. **3**, 181 (1981)

[6] B. Cabane, J. Phys. Chem. **81**, 1639 (1977)

[7] J. N. Turro, B. H. Barretz, and P. L. Kuo, Macromolecules **17**, 1321 (1984).

[8] K. Thalberg, B. Lindman, and K. Bergfeldt, Langmuir **7**, 2893 (1991).

[9] R. Nagarajan, Colloids Surf. **13**, 1 (1985).

[10] F. M. Witte and B. F. Engberts, Colloids Surf **36**, 417 (1989).

[11] P. Ilekti, T. Martin, B. Cabane, and L. Piculell, J. Phys. Chem. B **103**, 9831 (1999).

[12] P. Ilekti, L. Piculell, F. Tournilhac, and B. Cabane, J. Phys. Chem. B **102**, 344 (1998).

[13] M. Clerc, J. Phys. II (France) **6**, 961 (1996).

[14] M. Antonietti, J. Conrad, and A. Thunemann, Macromolecules **27**, 6007 (1994).

[15] E. A. Ponomarenko, A. J. Waddon, K. N. Bakeev, D. A. Tirrell, and W. J. MacKnight, Macromolecules **29**, 4340 (1996).

[16] P. Hansson, Langmuir **14**, 4059 (1998).

[17] S. Zhou, F. Yeh, C. Burger, and B. Chu, J.Phys.Chem.B **103**, 2107 (1999)

[18] D. Ruppelt, J. Kotz, W. Jaeger, S. E. Friberg, R. A. Mackay, Langmuir **13**, 3316 (1997).

[19] J. Merta, M. Torkkeli, T. Ikonen, R. Serimeaa, and P. Stenius, Macromolecules **34**, 2937 (2001).

[20] J. Merta, V. M. Garamus, A. I. Kuklin, R. Willumeit, and P. Stenius, Langmuir **16**, 10061 (2000).

[21] M. Dubois and Th. Zemb, J. Chem. Phys. **108**, 7855 (1998).

[22] G. Subramanian, R. P. Hjelm, T. J. Deming, G. S. Smith, Y. Li, and C. R. Safinya, J. Am. Chem. Soc. **122**, 26 (2000).

[23] E. A. Ponomarenko, A. J. Waddon, K. N. Bakeev, D. A. Tirrell, and W. J. Macknight, Macromolecules **29**, 4340 (1996).

[24] T. Salditt, I. Koltover, J. O. Raedler, and C. R. Safinya, Phys.Rev.E. **58**, 889 (1998).

[25] F. Artzner, R. Zantl, G. Rapp, and J. O. Raedler, Phys. Rev. Lett. **81**, 5015 (1998).

[26] Y. Hendrikx and J. Charvolin, J. Physique **42**, 1427 (1981).

[27] P. Kekicheff and B. Cabane, J. Physique **42**, 1427 (1981).

[28] K. Ghosh, G. A. Carri, M. Muthukumar, J. Chem. Phys. **115**, 4367 (2001).